

Torque-based Graph Surgery: Enhancing Graph Neural Networks with Hierarchical Rewiring

Sujia Huang¹, Lele Fu², Zhen Cui³, Tong Zhang^{1*}, Na Song⁴, Bo Huang¹

¹Nanjing University of Science and Technology, Nanjing, China

²Sun Yat-Sen University, Guangzhou, China

³Beijing Normal University, Beijing, China

⁴Putian University, FuZhou, China

hsujia2021@163.com, fulle@mail2.sysu.edu.cn

zhen.cui@bnu.edu.cn, tong.zhang@njust.edu.cn,

ptusn@ptu.edu.cn, huangbo@njust.edu.cn

Abstract

Graph Neural Networks (GNNs) have emerged as powerful tools for learning from graph-structured data, leveraging message passing to diffuse information and update node representations. However, most efforts have suggested that native interactions encoded in the graph may not be friendly for this process, motivating the development of graph rewiring methods. In this work, we propose a torque-driven hierarchical rewiring strategy, inspired by the notion of torque in classical mechanics, dynamically modulating message passing to improve representation learning in heterophilous graphs and enhance robustness against noisy graphs. Specifically, we define an interference-aware torque metric that integrates structural distance and energy scores to quantify the perturbation induced by edges, thereby encouraging each node to aggregate information from its nearest low-energy neighbors. We use the metric to hierarchically reconfigure each layer’s receptive field by judiciously pruning high-torque edges and adding low-torque links, suppressing propagation noise and boosting pertinent signals. Extensive evaluations on benchmark datasets show that our approach surpasses state-of-the-art methods on both heterophilous and homophilous graphs, and maintains high accuracy on noisy graph.

1 Introduction

Graph-structured data composed of vertices and edges encode entities and their relationships. Graph neural networks (GNNs) have emerged as a powerful framework for processing such data, with widespread applications in biomolecular modelling [1, 2], recommendation systems [3, 4] and beyond [5–7]. At the heart of GNNs lies message passing, which iteratively propagates and aggregates information along edges to enrich node representations. Therefore, the graph structure not only encodes entity interactions but also critically determines model performance [8–10].

In practice, however, raw graphs frequently harbour spurious or missing links arising from noise or sampling artefacts, compromising their effectiveness as substrates for message propagation. In response, recent work has devised diverse graph rewiring strategies that selectively remove and add edges to optimize message passing and boost predictive accuracy [11–14]. Such dynamic topology adjustment is crucial not only for mitigating noise but also for addressing heterophily, where nodes with dissimilar labels or features tend to be connected [15–17]. In such scenarios, homophily-based GNNs can be misled by abundant heterophilous connections, yielding entangled representations and degraded classification accuracy.

To explore the factors that influence message propagation for guiding effective rewiring, we simulate attacks by injecting adversarial edges into raw graphs and visualize the resulting structural perturbations. As shown in Figure 1(a)-(b), adversarial edges in the homophilous Cora span node pairs with larger feature distances than native connections. A similar trend is observed in Wisconsin that

inherently includes many heterophilous edges. To further uncover the attacker’s intention, we estimate node importance via the PageRank algorithm [18, 19] and derive an edge-level PageRank score by aggregating scores of each edge’s endpoints. As illustrated in Figure 1(c)-(d), adversarial edges exhibit two distinct patterns: in Cora, they preferentially connect high-PageRank nodes; whereas in Wisconsin, they appear predominantly among low-PageRank nodes, suggesting that PageRank cannot fully reveal the essence of adversarial edges. Moreover, real-world graphs inherently include spurious links even without external attacks, rendering PageRank insufficient to accurately assess the disruptive potential of edges. This motivates a key question: *can we jointly leverage structural distance and a more expressive metric of edge perturbation to achieve fine-grained graph refinement?*

We draw inspiration from the concept of **Torque** in classical mechanics, mathematically defined as the cross product of a lever arm (the position vector from the axis of rotation to the point of force application) and a force. Recently, torque has found utility in biology [20–22] and spintronics [23, 24]. Heuristically, we extend this concept to graphs by treating the distance between nodes as the lever arm and the noise exerted by a neighboring node on a central node as the force. Their product yields a graph torque, which measures an edge’s disruptive intensity: higher torque flags greater interference. To our knowledge, this is the first work to integrate a physics-inspired torque into graph rewiring, enabling an interference-aware message passing.

Specifically, we devise a Torque-driven Hierarchical Rewiring strategy (THR) for GNNs (TorqueGNN), which dynamically refines message passing to excel in both heterophilous and noisy graph. In THR, each edge is endowed with two learnable attributes: its Euclidean distance as the “lever arm”, which accentuates long-range or heterophilous links, and an energy score as the “force”, which is computed by its endpoints reflecting high values to noisy or noise-sensitive nodes and low values to benign ones. Their product defines a torque to quantify the interference strength of edges, where larger torques flag less reliable connections. Leveraging this metric, TorqueGNN hierarchically reconfigures each layer’s receptive field via automatically removing undesirable edges that result in performance degrading and introducing low-torque significant connections, thus effecting interference-resistant and importance-aware propagation. This rewiring is performed end-to-end, where message passing operates on the continuously updated graph, while the evolving node representations enhance torque computation.

Contributions: 1) To our knowledge, we are the first effort to apply the torque in physics into graph rewiring, culminating in TorqueGNN that enhances GNNs resilience to both heterophily and noise. 2) We devise a hierarchical rewiring strategy that adaptively infers each layer’s receptive field through automatically pruning undesirable connections and adding significant edges. 3) Comprehensive experiments indicate that TorqueGNN outperforms advanced GNNs across standard benchmarks and maintains robustness in noisy graphs, with THR surpassing superior rewiring strategies.

2 Related Work

Standard message passing in GNNs, which aggregates information from local neighbourhoods, struggles to capture long-range dependencies. A common remedy is to stack multiple layers to expand the receptive field [25–27], but this approach frequently encounters fundamental limitations such as over-smoothing and over-squashing. To address these bottlenecks, graph rewiring techniques have recently emerged as a powerful strategy to restructure connectivity and enhance information flow. For example, Expander GNNs and ExPhormer perform graph rewiring by merging multi-hop neighbourhoods or injecting virtual

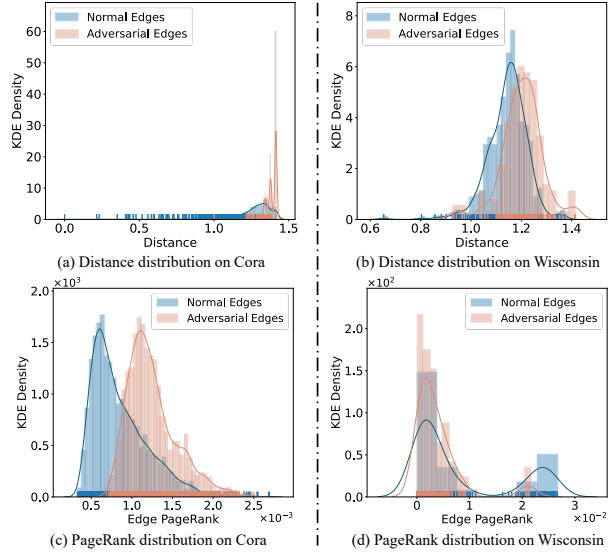


Figure 1: Density distributions of distances and PageRank scores for normal vs. adversarial edges on Cora and Wisconsin, where edge PageRank is the sum of endpoint scores in Cora and the absolute difference in Wisconsin.

nodes [28–30]. [31] adds edges based on spectral expansion to mitigate over-smoothing and over-squashing, while degree-preserving local edge-flip algorithms are developed [32]. [33, 34] analyze the root causes of over-squashing, demonstrating that both spatial and spectral rewiring can effectively counteract this bottleneck. Despite these advances, real-world graphs often remain inherently noisy, limiting the reliability of message passing.

Raw graph structures are frequently suboptimal substrates for message passing, as noisy edges and perturbed features can induce both spurious and missing links, thereby limiting the expressive power of GNNs [33, 35]. To mitigate the effect of such undesirable connections, [36] simultaneously perform graph rewiring and feature denoising to boost classification accuracy. Moreover, [36] highlights the challenge posed by heterophilous edges, wherein the aggregation of dissimilar node signals can lead to entangled representations and misclassifications. There are many methods specifically devised for heterophily. For example, [37–39] employ signed message propagation, assigning positive weights to homophilous links and negative weights to heterophilous ones. This enables differentiated updates on the heterophilous graphs, thereby amplifying similarity among homophilous nodes while suppressing similarity among heterophilous ones. However, [40] has shown that, although single-hop signed adjacency matrix aids in distinguishing features of different classes, the multi-hop propagation matrix introduced to expand the receptive field often degrades performance.

We are inspired by the torque in physics to design a new rewiring mechanism that hierarchically eliminates undesirable connections and incorporates task-relevant edges. By dynamically reshaping the receptive field during training, our method enhances the discriminative power of GNNs in noisy and heterophilous graphs.

3 Preliminaries

3.1 Notations

Let us define an undirected graph dataset as $\mathcal{G} = (V, \mathcal{E})$, comprising N nodes $\{v_i \in V\}_{i=1}^N$ and K edges $\{e_k \doteq \langle i, j \rangle \in \mathcal{E}\}_{k=1}^K$, where each edge k encodes a connection between nodes v_i and v_j . We denote the adjacency matrix by $\mathbf{A} \in \{0, 1\}^{N \times N}$, where $A_{\langle i, j \rangle} = 1$ iff nodes v_i and v_j are connected, 0 otherwise. Furthermore, $\hat{\mathbf{A}} = \mathbf{A} + \mathbf{I}$ indicates \mathbf{A} with added self-loops, and $\tilde{\mathbf{A}} = \hat{\mathbf{D}}^{-1/2} \hat{\mathbf{A}} \hat{\mathbf{D}}^{-1/2}$ denotes the symmetrically normalized adjacency matrix with $\hat{D}_{\langle i, i \rangle} = \sum_{j=1}^N \hat{A}_{\langle i, j \rangle}$. Each node is associated with a feature vector, and we write $\mathbf{X} \in \mathbb{R}^{N \times d}$ for the node feature matrix, where the i -th row $\mathbf{x}_i \in \mathbb{R}^d$ represents the d -dimensional features of node v_i . Among N nodes, N_{lab} nodes are labeled, with ground-truth labels encoded in a matrix $\mathbf{Y} \in \mathbb{R}^{N_{lab} \times c}$, where each row \mathbf{y}_i is a one-hot vector indicating the class label among c categories.

3.2 Message Passing

Consider a graph with adjacency matrix \mathbf{A} and node feature matrix \mathbf{X} . Message passing in a GNN proceeds by iteratively propagating and aggregating neighborhood information as

$$\mathbf{h}_i^{(l+1)} = \text{Upd}(\mathbf{h}_i^{(l)}, \sum_{v_j \in \mathcal{N}_i} \text{Agg}(\mathbf{h}_j^{(l)}, A_{\langle i, j \rangle})), \quad (1)$$

where $\mathbf{h}_i^{(0)} = \mathbf{x}_i$, and $\mathbf{h}_i^{(l+1)} \in \mathbb{R}^m$ is the representation of node v_i in the $(l+1)$ -th layer. $\text{Agg}(\cdot)$ computes the incoming message from a neighbor v_j , and $\text{Upd}(\cdot)$ updates the representation of node v_i . Rather than relying on the raw adjacency matrix \mathbf{A} , most GNNs adopt a modified propagation operator \mathcal{A} . For example, [41] replaces each non-zero entry of \mathbf{A} with a learned attention coefficient that depends on the representations of the corresponding node pair.

3.3 Energy-based Model

Energy-based model (EBM) [42] aims to establish an energy function $E(\mathbf{x}, y) : \mathbb{R}^d \rightarrow \mathbb{R}$, which maps an input instance \mathbf{x} with a given label y to a scalar value termed energy. Consequently, the Boltzmann

distribution is expressed as

$$p(y|\mathbf{x}) = \frac{\exp(-E(\mathbf{x}, y))}{\sum_{y'} \exp(-E(\mathbf{x}, y'))} = \frac{\exp(-E(\mathbf{x}, y))}{\exp(-E(\mathbf{x}))}, \quad (2)$$

where the denominator $\sum_{y'} \exp(-E(\mathbf{x}, y'))$ is the partition function. [43, 44] connect neural classifiers $f(\cdot)$, which map an input to a c -dimensional logit vector, with energy-based models by setting the energy as the negative logit value of the classifier $E(\mathbf{x}, y) = -f(\mathbf{x})[y]$, where $f(\mathbf{x})[y]$ denotes the non-normalized logit corresponding to class y . Then, the energy of the input instance marginalizing over all possible labels becomes

$$E(\mathbf{x}) = -\log \sum_{y'} \exp(-E(\mathbf{x}, y')) = -\log \sum_{y'} \exp(f(\mathbf{x})[y']). \quad (3)$$

4 Methodology

In this section, we propose a novel graph rewiring strategy that unfolds in three key stages: (i) computing edge torques, (ii) rewiring propagation matrix, and (iii) adjusting message passing. The full algorithmic pseudocode is provided in Appendix A, while a detailed complexity analysis of TorqueGNN is included in Appendix B.

4.1 Derive Graph Torque

In classical mechanics, *torque* is defined as the vector cross product of a force and its lever arm:

$$\mathbf{T} = \mathbf{r} \times \mathbf{F}, \quad |\mathbf{T}| = |\mathbf{r}| |\mathbf{F}| \sin \theta, \quad (4)$$

where \mathbf{r} denotes the lever arm vector connecting the point of application to the axis of rotation, \mathbf{F} indicates the force vector, and θ is the angle between them. The magnitude of the torque directly governs an object’s tendency to rotate under the applied force. In GNNs, the systematic exploration of node interactions mirrors the lever arm–force relationship underlying torque in classical mechanics. Specifically, we can transpose torque to graphs by treating the distance $D_{\langle i, j \rangle}$ between a central node v_i and its neighbor v_j as a scalar “lever arm”, and the neighbor’s influence level $E_{\langle i, j \rangle}$ as a scalar “disturbing force” on v_i . In graphs, the notion of a disturbing force is abstract and lacks a well-defined direction, as message passing in GNNs does not involve physical “rotation” in the classical mechanical sense. Therefore, rather than computing the full vector torque via a cross product, we adopt a scalar approximation based on the product of distance and energy. Mathematically, for the edge k connecting nodes v_i and v_j , we define its torque value as follow,

$$T_{e_k} = D_{\langle i, j \rangle} \times E_{\langle i, j \rangle}, \quad (5)$$

which measures the disturbance strength that the message carried by edge e_k imposes on node v_i . Obviously, larger distances or higher disturbance both amplify torque, while edges maximizing both factors yield the greatest torque that represents the highest priority for graph rewiring. Crucially, the definition of D and, in particular, E in Eq. (5), remains a key challenge for accurate rewiring. Here, we employ an EBM to quantify node interference, and subsequently delineate the construction of both D and E .

Metric 1: Distance. To mitigate the effect of noise in raw graphs and features, we estimate node distances using optimized representations. Specifically, for a central node v_i and its neighbor v_j , we have the following formulation

$$D_{\langle i, j \rangle} = \|\mathbf{h}_i - \mathbf{h}_j\|_2, \quad (6)$$

where $\mathbf{h}_i = \text{gCov}(\mathbf{x}_i, \mathbf{A}; \Theta)^1$ denotes the representation of v_i obtained via a graph convolution operator “gCov” parameterized by Θ and followed by a ReLU activation.

Metric 2: Energy. While graph-based message passing can markedly enhance node representations, it also risks amplifying structural and feature noise. To mitigate this, we posit nodes that persistently

¹ “gCov” can be instantiated with any standard GNN layer, such as GCN, GAT, or APPNP; in this work, we adopt APPNP as our backbone.

absorb noisy signals exhibit elevated interference strength relative to benign nodes. EBM, which assigns scalar energy values to inputs and has demonstrated remarkable robustness against adversarial perturbations [45, 46], provide a foundation for this purpose. Therefore, we introduce an EBM-derived energy score as another indicator of edge reliability, as shown in Eq. (3), which assigns low energy to benign samples and high energy to corrupted ones. In our framework, an energy-based GNN jointly performs node classification and energy estimation. For a network parameterized by Θ , the energy of node v_i is defined as $E_{\Theta}(\mathbf{x}_i) = -\log \sum_y \exp(\mathbf{h}_i[y])$. Here, \mathbf{h}_i denotes the logit vector for node v_i . We then derive an edge-level energy metric by combining the energy scores of node pairs,

$$E_{\langle i,j \rangle} = E_{\Theta}(\mathbf{x}_i) \times E_{\Theta}(\mathbf{x}_j). \quad (7)$$

4.2 Adjust Message Passing

Edge-removal High-order Rewiring. Herein, we propose an automated threshold learning mechanism that identifies the optimal number of edges to prune by pinpointing the largest successive torque gap. Specifically, we first rank all K edges in descending order of their torque values to form a torque-sorted list (TSL), denoting its k -th entry as \tilde{e}_k with torque \tilde{T}_{e_k} , so that $\tilde{T}_{e_1} \geq \tilde{T}_{e_2} \geq \dots \geq \tilde{T}_{e_K}$. We then calculate the torque gap between two consecutive links by

$$G_{k,k+1} = \mu_k \times \frac{\tilde{T}_{e_k}}{\tilde{T}_{e_{k+1}} + \delta}, \quad (8)$$

where δ is a small constant to prevent division by zero, and the weight μ_k reflects the proportion of anomalous edges, those whose distance D , energy E and torque T all exceed their respective means, that are captured within the top k torque-ranked set, emphasizing the boundary between desirable and undesirable connections. The computation formula of μ_k is defined as

$$\begin{aligned} \mu_k &= \frac{|High_e \cap Top_k|}{|High_e|}, \\ High_e &= \{e_k \doteq \langle i, j \rangle | D_{\langle i, j \rangle} \geq \bar{D}, E_{\langle i, j \rangle} \geq \bar{E}, T_{\langle i, j \rangle} \geq \bar{T}, \langle i, j \rangle \in \mathcal{E}\}, \\ Top_k &= \{e_k \doteq \langle i, j \rangle | Top_k\{T_{\langle i, j \rangle}\}, \langle i, j \rangle \in \mathcal{E}\}, \end{aligned} \quad (9)$$

where $\bar{D}, \bar{E}, \bar{T}$ denote the mean values of distance, energy and torque, respectively, computed over all K edges. The set $High_e$ comprises edges exhibiting above-average values across all three metrics, while Top_k contains the top k connections in TSL. According to (8), we can identify the optimal cutoff by locating the largest torque gap $\mathcal{K} = \arg \max_{0 \leq k \leq K-1} G_{k,k+1}$, which separates the edge set into two groups: undesirable connections ($\tilde{e}_1, \dots, \tilde{e}_{\mathcal{K}}$) and desirable connections ($\tilde{e}_{\mathcal{K}+1}, \dots, \tilde{e}_K$).

In practice, multi-layer GNNs, such as APPNP [47], are widely adopted to enlarge the receptive field of graph convolutions. Building on the pairwise torque gap formulation introduced above, we extend this mechanism across multiple propagation layers. In specific, for each order l , we construct a dedicated propagation matrix that enables selective filtering of undesirable high-order interactions. Let $\mathcal{A}^{(l)}$ denote the refined propagation matrix used in l -th layer and $\mathcal{A}^{(0)} = \mathbf{A}$. We have current neighbors v_j of a given node v_i based on $\mathcal{A}^{(l)}$, and recompute two key properties as follows

$$D_{\langle i,j \rangle}^{(l+1)} = \|\mathbf{h}_i^{(l)} - \mathbf{h}_j^{(l)}\|_2, \quad E_{\langle i,j \rangle}^{(l+1)} = E_{\Theta}^{(l)}(\mathbf{x}_i) \times E_{\Theta}^{(l)}(\mathbf{x}_j), \quad (10)$$

where $l = 0, \dots, L-1$, and $E_{\Theta}^{(l)}(\mathbf{x}_i) = -\log \sum_y \exp(\mathbf{h}_i^{(l)}[y])$. The initial representation $\mathbf{h}_i^{(0)} = \mathbf{x}_i \Theta$ is computed via a linear transformation of the input feature \mathbf{x}_i . Consequently, we gain the $(l+1)$ -th order torque $T^{(l+1)}$ and the corresponding gap $G^{(l+1)}$ using Eqs. (5)-(9), thereby deriving a pruned propagation matrix $\mathcal{A}^{(l+1)*}$ with $(K - \mathcal{K})$ non-zero elements.

Edge-addition High-order Rewiring. In the previous steps, we identify undesirable high-order neighbors by computing the torque of existing edges based on two key attributes. Extending this strategy, we also consider expanding the receptive field by adding edges that are initially absent but potentially beneficial for message passing. However, evaluating torque across all missing edges is computationally intractable, so that we construct a candidate set \mathcal{T} by selecting, for each node, its top- t most similar peers. We then compute the $(l+1)$ -th order torque $T^{(l+1)}$ for the resulting $N \times t$ candidate edges, and

select $r \times N \times t$ edges with the lowest torque values, where r is a sampling ratio. Nevertheless, this hard selection process is inherently non-differentiable and thus cannot be used in gradient-based optimization. To overcome this, we adopt the Gumbel-Softmax reparameterization trick [45], which enables differentiable sampling by approximating discrete decisions with a continuous relaxation. For each candidate edge k , we define its logits $\boldsymbol{\pi}_k = [\pi_{k0}, \pi_{k1}]$, where $\pi_{k0} = T_{e_k}^{(l+1)}$ (discard) and $\pi_{k1} = 1 - T_{e_k}^{(l+1)}$ (select). Drawing independent noise $g_{kj} \sim \text{Gumbel}(0, 1)$, the soft selection probabilities are computed via

$$p_{kj} = \frac{\exp\left(\frac{\log(\pi_{kj}) + g_{kj}}{\tau}\right)}{\sum_{m=1}^2 \exp\left(\frac{\log(\pi_{km}) + g_{km}}{\tau}\right)}, \forall j = 0, 1, k \in \{1, 2, \dots, N \times t\}, \quad (11)$$

where τ is a temperature parameter controlling the sharpness of the Gumbel-Softmax distribution. p_{k1} serves as a differentiable weight indicating the likelihood of selecting candidate edge k . Finally, we construct the rewired propagation matrix $\mathcal{A}^{(l+1)}$ by augmenting $\mathcal{A}^{(l+1)*}$ with these probabilistically weighted candidate edges, followed by the standard renormalization procedure.

Messaging Passing on Rewired Graph. By rewiring the adjacency matrix \mathbf{A} as described, each propagation layer is endowed with an expanded receptive field capable of capturing effective high-order interactions while suppressing noise. Let $\mathcal{N}_i^{(l+1)} = \{v_j | \mathcal{A}_{(i,j)}^{(l+1)} \neq 0\}$ denotes the refined $(l+1)$ -hop neighborhood of node v_i . The message passing in the $(l+1)$ -th layer is defined as

$$\mathbf{h}_i^{(l+1)} = \text{ReLU}\left(\sum_{j \in \{v_i\} \cup \mathcal{N}_i^{(l+1)}} \alpha \mathbf{h}_j^{(l)} + (1 - \alpha) \mathbf{h}_i^{(0)}\right). \quad (12)$$

The final node representations from the last layer are fed into a fully connected layer parameterized by $\Phi \in \mathbb{R}^{m \times c}$ to yield the predicted class probabilities. These predictions are compared against the ground-truth labels using a cross-entropy loss minimized through gradient-based optimization.

4.3 Energy Calibration Objective

The energy function represents the unnormalized negative log-likelihood of node v_i , where a lower energy corresponds to a higher likelihood and, consequently, a greater probability of the sample being benign. In EBMs, the fundamental objective is to assign low energy to positive samples and high energy to others, thereby maximizing the likelihood of the observed data. This is typically achieved by minimizing the negative log-likelihood, formulated as

$$\mathcal{L} = -\frac{1}{N} \sum_{i=1}^N \log p_{\Theta}(\mathbf{x}_i). \quad (13)$$

Here, $p_{\Theta}(\mathbf{x}) = \frac{\exp(-E_{\Theta}(\mathbf{x}))}{Z_{\Theta}}$ is a probabilistic model with the partition function $Z_{\Theta} = \int \exp(-E_{\Theta}(\mathbf{x})) d\mathbf{x}$. However, directly optimizing the above negative log-likelihood is often infeasible due to the challenge of computing Z_{Θ} . To this end, score matching [48] provides an effective alternative. Rather than relying on the likelihood, score matching estimates the parameters by aligning the gradients (scores) of the model's log-density with those of the empirical data distribution $p_{data}(\mathbf{x})$, avoiding the estimation of Z_{Θ} . Its objective seeks to minimize the following discrepancy between the model and data distributions

$$\mathcal{F}(p_{data}(\mathbf{x}) || p_{\Theta}(\mathbf{x})) = \mathbb{E}_{p_{data}(\mathbf{x})} \left[\frac{1}{2} \|\nabla_{\mathbf{x}} \log p_{data}(\mathbf{x}) - \nabla_{\mathbf{x}} \log p_{\Theta}(\mathbf{x})\|^2 \right]. \quad (14)$$

To enlarge the energy signal of undesirable connections to facilitate more clearer distinction during edge selection, inspired by [46], we generate negative examples by randomly perturbing the graph structure, i.e., by adding or removing edges. Let $\hat{E}_{\Theta}(\mathbf{x}_i)$ denote the energy of node v_i on this perturbed graph. We then define an energy-based score according to the following definition

Definition 1 (Energy Score): For a node v_i , its score $S_{\Theta}(\mathbf{x}_i)$ assigned by the energy model is surrogated by a gradient in the discrete space:

$$S_{\Theta}(\mathbf{x}_i) = \nabla_{\mathbf{x}_i} E_{\Theta}(\mathbf{x}_i) = \left[\frac{E_{\Theta}(\mathbf{x}_1) - \hat{E}_{\Theta}(\mathbf{x}_1)}{E_{\Theta}(\mathbf{x}_1)}, \dots, \frac{E_{\Theta}(\mathbf{x}_M) - \hat{E}_{\Theta}(\mathbf{x}_M)}{E_{\Theta}(\mathbf{x}_M)} \right], \quad (15)$$

where M is the number of perturbed samples used. In fact, since $-\log p_{\Theta}(\mathbf{x}) = E_{\Theta}(\mathbf{x})$, Eq. (15) equals to the following formula,

$$S_{\Theta}(\mathbf{x}_i) = \nabla_{\mathbf{x}_i} E_{\Theta}(\mathbf{x}_i) = \left[\frac{\log p_{\Theta}(\mathbf{x}_1) - \log \hat{p}_{\Theta}(\mathbf{x}_1)}{\log p_{\Theta}(\mathbf{x}_1)}, \dots, \frac{\log p_{\Theta}(\mathbf{x}_M) - \log \hat{p}_{\Theta}(\mathbf{x}_M)}{\log p_{\Theta}(\mathbf{x}_M)} \right]. \quad (16)$$

Due to the energy score surrogate, the objective (14) of score matching is reformulated as follows

$$\mathcal{F}(p_{data}(\mathbf{x}_i) \| p_{\Theta}(\mathbf{x}_i)) = \mathbb{E}_{p_{data}(\mathbf{x}_i)} \left[\frac{1}{2} \|S_{data}(\mathbf{x}_i) - S_{\Theta}(\mathbf{x}_i)\|^2 \right]. \quad (17)$$

However, the real data is unavailable during training, and thus following [46, 49] and Definition 1, the final optimization formula is given by

$$\mathcal{L}_{sm} = \frac{1}{N} \sum_{i=1}^N \left[\nabla_{\mathbf{x}_i} S_{\Theta}(\mathbf{x}_i)^{\top} \nabla_{\mathbf{x}_i} S_{\Theta}(\mathbf{x}_i) + \frac{1}{2} \|S_{\Theta}(\mathbf{x}_i)\|^2 \right]. \quad (18)$$

By minimizing the surrogate loss (18), we not only approximate the original score matching objective of the EBM, but also explicitly amplify the energy signals associated with undesirable edges.

5 Experiments

Datasets. We evaluate our method on ten standard node classification benchmarks, including three homophilous graphs (Citeseer, Cora, and Pubmed) and seven heterophilous graphs (Texas, Wisconsin, Cornell, Actor, Tolokers, Questions, and Penn94). Among them, Tolokers, Questions, and Penn94 are large-scale datasets. Following previous work, we adopt the same data split strategy: 48% of the nodes are used for training, 32% for validation, and the remaining 20% for testing. The statistics of these datasets are summarized in Table 1, and further details can be found in Appendix C.2.

Competitors. To evaluate the effectiveness of our model in capturing high-order interactions, we adopt APPNP as the downstream GNN, due to its suitability for deep graph architectures. We compare our approach against eleven baselines: a two-layer MLP; three classic homophily-oriented GNNs, including GCN [50], GAT [41] and APPNP [47]; and seven representative methods specifically designed for heterophilous graphs: H₂GCN [51], GPR-GNN [52], FAGCN [39], ACM-GCN [38], OGNN [53], M2M-GNN [40], PCNet [54]. Furthermore, to assess the impact of our THR rewiring strategy, we compare it with other rewiring strategies: first-order spectral rewiring (FoSR) [55], joint denoising and rewiring (JDR) [36] and randomly removing edges (DropEdge) [56]. More details on all methods are provided in Appendix C.3.

Table 1: Benchmark dataset statistics.

| Datasets | Edge Hom. | #Nodes | #Edges | #Classes | #Features |
|-----------|-----------|--------|-----------|----------|-----------|
| Texas | 0.11 | 183 | 295 | 5 | 1,703 |
| Wisconsin | 0.21 | 251 | 466 | 5 | 1,703 |
| Cornell | 0.30 | 183 | 280 | 5 | 1,703 |
| Actor | 0.22 | 7,600 | 26,752 | 5 | 931 |
| Tolokers | 0.60 | 11,758 | 51,900 | 2 | 10 |
| Questions | 0.84 | 48,921 | 153,540 | 2 | 301 |
| Penn94 | 0.47 | 41,554 | 1,362,229 | 2 | 4,814 |
| Citeseer | 0.74 | 3,327 | 4,676 | 7 | 3,703 |
| Cora | 0.81 | 2,708 | 5,278 | 6 | 1,433 |
| Pubmed | 0.80 | 19,717 | 44,327 | 3 | 500 |

Setups. We report node classification ACC, defined as the proportion of correctly predicted labels. For most benchmark datasets, models are trained using the Adam optimizer for 100 epochs with a learning rate of 0.001 and 512 hidden units. For larger datasets such as Tolokers, Questions, and Penn94, the number of training epochs is increased to 500 to ensure sufficient training. Detailed hyperparameter and environment configurations are provided in Appendix C.4, including the code link in C.1. Each experiment is repeated ten times, and we report the mean and standard deviation.

Node Classification Results. Table 2 reports test-set accuracy for three TorqueGNN variants, including edge-addition THR (A-THR), edge-removal THR (R-THR) and mixed THR (M-THR), alongside eleven state-of-the-art baselines across seven benchmark datasets. Several insights emerge: 1) On every dataset, at least one TorqueGNN variant appears among the top three performers, and TorqueGNN achieves the

Table 2: Node classification results on benchmark datasets: Mean ACC % \pm Standard Deviation %. The first-, second- and third-best accuracy are highlighted in **red**, **green** and **blue**, respectively.

| Methods | Citeseer | Cora | Pubmed | Texas | Wiscon. | Cornell | Actor |
|---------------------------|----------------------------------|----------------------------------|----------------------------------|----------------------------------|----------------------------------|----------------------------------|----------------------------------|
| MLP | 74.02 \pm 1.90 | 75.69 \pm 2.00 | 87.16 \pm 0.37 | 80.81 \pm 4.75 | 85.29 \pm 3.31 | 81.89 \pm 6.40 | 36.53 \pm 0.70 |
| GCN | 76.50 \pm 1.36 | 86.98 \pm 1.27 | 88.42 \pm 0.50 | 55.14 \pm 5.16 | 51.76 \pm 3.06 | 60.54 \pm 5.30 | 27.32 \pm 1.10 |
| GAT | 76.55 \pm 1.23 | 87.30 \pm 1.10 | 86.33 \pm 0.48 | 52.16 \pm 6.63 | 49.41 \pm 4.09 | 61.89 \pm 5.05 | 27.44 \pm 0.89 |
| H ₂ GCN | 77.11 \pm 1.57 | 87.87 \pm 1.20 | 89.49 \pm 0.38 | 84.86 \pm 7.23 | 87.65 \pm 4.98 | 82.70 \pm 5.28 | 35.70 \pm 1.00 |
| GPR-GNN | 77.13 \pm 1.67 | 87.95 \pm 1.18 | 87.54 \pm 0.38 | 78.38 \pm 4.36 | 82.94 \pm 4.21 | 80.27 \pm 8.11 | 34.63 \pm 1.22 |
| FAGCN | 74.01 \pm 1.85 | 86.34 \pm 0.67 | 76.57 \pm 1.88 | 77.56 \pm 6.11 | 79.41 \pm 6.55 | 78.64 \pm 5.47 | 34.85 \pm 1.61 |
| ACM-GCN | 77.32\pm1.70 | 87.91 \pm 0.95 | 90.00 \pm 0.52 | 87.84 \pm 4.40 | 88.43 \pm 3.22 | 85.14 \pm 6.07 | 36.28 \pm 1.09 |
| OGNN | 77.31 \pm 1.73 | 88.37 \pm 0.75 | 90.15\pm0.38 | 86.22 \pm 4.12 | 88.04 \pm 3.63 | 87.03\pm4.73 | 37.99\pm1.00 |
| M2M-GNN | 77.20 \pm 1.80 | 88.12\pm1.00 | 90.35\pm0.60 | 89.19\pm4.50 | 89.01\pm4.10 | 86.48 \pm 6.10 | 36.72 \pm 1.60 |
| PCNet | 77.50\pm1.06 | 88.41\pm0.66 | 89.51 \pm 0.28 | 88.11 \pm 2.17 | 88.63\pm2.75 | 82.61 \pm 2.70 | 37.80\pm0.64 |
| APPNP (<i>backbone</i>) | 74.02 \pm 0.38 | 88.32 \pm 0.41 | 84.53 \pm 0.34 | 49.17 \pm 3.30 | 47.60 \pm 4.54 | 55.83 \pm 4.02 | 29.03 \pm 1.12 |
| TorqueGNN w M-THR | 75.86 \pm 0.23 | 84.78 \pm 0.28 | 87.52 \pm 0.06 | 91.11\pm1.67 | 89.60\pm1.20 | 89.44\pm1.67 | 36.72\pm0.16 |
| TorqueGNN w R-THR | 76.51 \pm 0.09 | 86.73 \pm 0.50 | 90.18\pm0.24 | 88.61\pm0.83 | 86.20 \pm 0.60 | 90.83\pm2.50 | 36.07 \pm 0.36 |
| TorqueGNN w A-THR | 78.03\pm0.05 | 88.47\pm0.28 | 89.38 \pm 0.02 | 86.11 \pm 0.01 | 82.00 \pm 0.01 | 83.61 \pm 3.15 | 36.24 \pm 0.04 |

highest accuracy on the majority of benchmarks. 2) Three rewiring strategies yield substantial gains over APPNP and improvements are most pronounced on heterophilous graphs, underscoring the significance of our torque-based rewiring. 3) On Citeseer, Cora, and Pubmed, both A-THR and R-THR outperform the M-THR variant, suggesting that simultaneous addition and removal can inadvertently constrain information flow for citation networks. 4) In highly heterophilous datasets, although edge addition boosts APPNP, original undesirable links limit its effect. By contrast, R-THR achieves more high accuracy by judiciously deleting these connections. 5) In cases such as Pubmed and Cornell, R-THR attains the best results, likely because aggressive removal of noisy original edges without introducing additional candidates yields a cleaner propagation structure.

Table 3: Node classification results on **large-scale** datasets: Mean ACC % (ROC AUC for imbalanced Questions) \pm Standard Deviation %, where the optimal and suboptimal results are highlighted in **red** and **green**, respectively.

| | Penn94 | Tolokers | Questions |
|----------|---------------------|---------------------|---------------------|
| baseGNN | 75.19 (0.17) | 76.47 (1.16) | 46.57 (0.71) |
| FoSR | 75.21 (0.19) | 76.64 (1.15) | 46.95 (0.83) |
| JDR | 75.19 (0.23) | 78.06 (0.88) | 46.98 (0.87) |
| DropEdge | 78.46 (0.02) | 77.03 (0.26) | 60.01 (0.24) |
| THR | 80.88 (0.01) | 78.08 (0.16) | 62.64 (0.89) |

FoSR and JDR achieve only marginal gains. Moreover, THR surpasses DropEdge, validating the effectiveness of the proposed torque-driven manner.

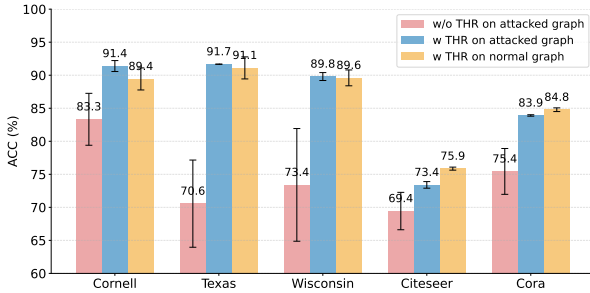


Figure 2: Results of TorqueGNN w/o THR and w THR on graphs with noisy edges.

Results on Larger Graphs. Scalability of rewiring techniques on large graphs is crucial, particularly for end-to-end methods that dynamically add and remove edges during training. In TorqueGNN, the principal computational burden stems from computing high-order torques and corresponding gaps, which incurs a complexity of $\mathcal{O}(|\mathcal{A}^{(l)}| \log |\mathcal{A}^{(l)}|)$ (see Appendix B for details). Despite this overhead, THR remains tractable for large graphs. Table 3 compares multiple rewiring schemes on larger heterophilous datasets: Both THR and DropEdge yield substantial accuracy improvements over the base GNN, yet THR consistently outperforms all alternatives. In contrast,

Results on Adversarially Perturbed Graphs.

Our torque-driven rewiring not only improves predictive accuracy but also enhances robustness to structural attacks by detecting and suppressing adversarial edges. To evaluate this, we employ MetaAttack [57] to inject adversarial links at a perturbation rate of 25% of the original edge count. Figure 2 compares classification accuracy under three settings: TorqueGNN without THR (w/o THR) on attacked graph, TorqueGNN with THR (w THR) on attacked graph and TorqueGNN w THR on normal graph. In all cases, we employ the mixed addition and deletion strategy for optimization. As shown, across both homophilous and heterophilous datasets, applying THR to the

perturbed graph substantially improves classification performance, which demonstrates the effectiveness of our method in detecting and eliminating adversarial edges. Moreover, on heterophilous datasets, TorqueGNN w THR applied to the attacked graph even surpasses its performance on the normal graph, suggesting that the injected adversarial edges accentuate the distinction between desirable and undesirable connections, thereby enhancing the effectiveness of our rewiring mechanism.

Ablation Study. Table 2 has shown that all three THR variants markedly improve upon the APPNP backbone. To evaluate their broader applicability, we incorporate each strategy into two classic two-layer GNNs (GCN and GAT), and repeat the ablation studies in Figure 3. As illustrated, on the highly heterophilous Texas, Wisconsin, and Actor datasets, every rewiring variant substantially outperforms its base GNN. Even on the homophilous Pubmed, R-THR surpasses the base models, echoing the results in Table 2 and underscoring the broad applicability of our torque-driven optimization. We note, however, that A-THR and M-THR occasionally underperform relative to the baselines, likely because the current structure is already well-formed, and excessive edge additions may introduce noise, thereby degrading classification performance. Ablation study of significant components is included in Appendix C.5.

Parameter Analysis. To assess the influence of the key hyperparameter α , we perform a sensitivity analysis shown in Figure 4. The figure examine the trade-off parameter α , which balances the contribution of the learned hidden representation and the original input features, where a larger α increases the influence of the hidden representations. We observe that smaller graphs (e.g., Texas and Cornell), optimal accuracy is achieved at low α value ($0.01 \leq \alpha \leq 0.05$), implying that raw node features provide sufficient discriminative power. In contrast, on medium-to-large graphs, better performance is observed when $\alpha \geq 0.5$, reflecting the necessity of high-order hidden representations to capture more complex community structures. Sensitivity analysis of other hyperparameters is presented in Appendix C.5.

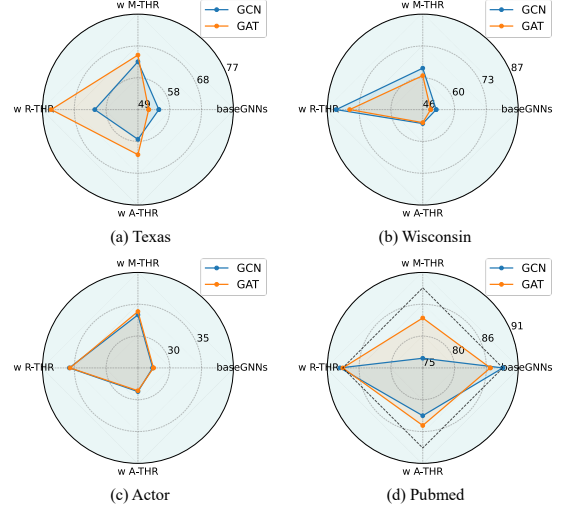


Figure 3: Ablation study: Performance comparison of GCN and GAT with different rewiring schemes on four datasets.

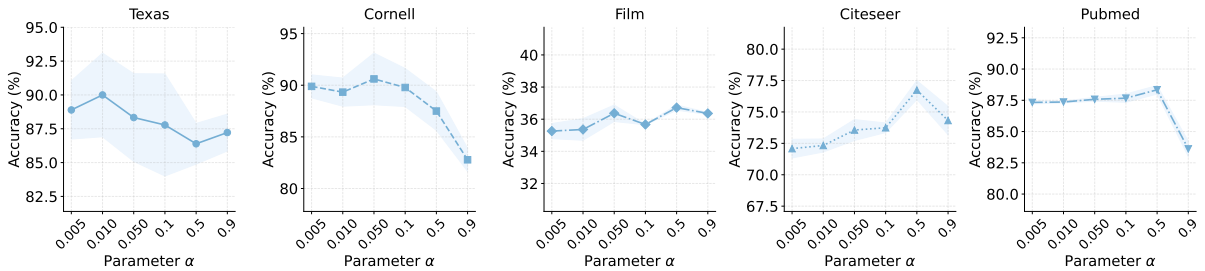


Figure 4: Parameter sensitivity: Performance curves on five datasets with ranging α in $\{0.005, \dots, 0.9\}$.

6 Conclusion

In summary, we proposed a **Torque**-driven hierarchical rewiring graph neural network (**TorqueGNN**), which dynamically refined the graph structures to enhance representation learning on heterophilous and noisy graphs. By introducing an interference-aware torque metric, the product of the distance and the energy between node representations, TorqueGNN automatically removed undesirable connections and introduced beneficial ones during message passing. This hierarchical rewiring yielded interference-resilient, importance-aware propagation tailored to each layer’s receptive field. Extensive evaluations across homophilous and heterophilous benchmark datasets demonstrated that TorqueGNN consistently outperformed state-of-the-art baselines and maintained robust performance on adversarial graphs. We state the

limitations of our model in Appendix D.

A Algorithm

Algorithm 1 outlines the complete workflow of TorqueGNN.

| | |
|--|---|
| Algorithm 1: TorqueGNN | |
| Input: Node features $\{\mathbf{x}_i \in \mathbb{R}^d\}_{i=1}^N$, candidate edge set \mathcal{T} , ground truth matrix \mathbf{Y} , hyperparameters L and α . | |
| Output: The predicted class label. | |
| 1 | Initialize network parameters Θ, Φ ; |
| 2 | $\mathbf{h}_i^{(0)} = \text{ReLU}(\mathbf{x}_i \Theta)$; |
| 3 | for $l = 1 \rightarrow L$ do |
| 4 | ▷ Forward Propagation |
| 5 | Compute pairwise distance $D_{\langle i,j \rangle}^{(l)}$ and energy $E_{\langle i,j \rangle}^{(l)}$ with Eqs. (6) and (7); |
| 6 | Compute the l th order torques with Eq. (5) and sort them. // Torque computation |
| 7 | Gain the largest torque gap \mathcal{K} with Eqs. (8)-(9); |
| 8 | Remove the top \mathcal{K} edges to gain $\mathcal{A}^{(l)*}$. // Removing undesirable edges |
| 9 | Compute the sampling probability of candidate edges with Eq. (11); |
| 10 | Add beneficial candidate edges to form the refined propagation matrix $\mathcal{A}^{(l)}$. // Adding desirable connections |
| 11 | Update node representation $\mathbf{h}_i^{(l)}$ with Eq. (12). // Message passing |
| 12 | ▷ Backward Propagation |
| 13 | Classifier $f(\cdot) \leftarrow \text{LocalUpdating}(\mathbf{x}_i, \{\mathcal{A}^{(l)}\}_{l=1}^L)$ with the cross-entropy loss // Standard training |
| 14 | for $t = 1 \rightarrow T$ do |
| 15 | $f^{(t+1)}(\cdot) \leftarrow \text{EnergyCalibrating}(f^t(\cdot), \mathbf{x}_i, \{\mathcal{A}^{(l)}\}_{l=1}^L)$ with Eq. (18) // Energy calibration |
| 16 | Obtain $\hat{\mathbf{y}}_i = \text{Softmax}(\mathbf{h}_i^{(L)} \Phi)$; |
| 17 | return The predicted class label of the i -th node is given by $\arg \max \hat{\mathbf{y}}_i$. |

B Complexity Analysis

The dominant computational cost of TorqueGNN lies in: 1) Torque computation and graph rewiring. For each order l , we compute torque values only on the edges in $\mathcal{A}^{(l)}$, costing $\mathcal{O}(|\mathcal{A}^{(l)}|)$, and then sort these values in $\mathcal{O}(|\mathcal{A}^{(l)}| \log |\mathcal{A}^{(l)}|)$. When adding edges, if the candidate set size is B , the combined probability calculation and sorting cost is $\mathcal{O}(B + B \log B)$. 2) Message passing on the rewired graph $\mathcal{A}^{(l)}$. Initial representations $\mathbf{H}^{(0)}$ are obtained by a fully connected layer with parameter $\Theta \in \mathbb{R}^{d \times m}$ on $\mathbf{X} \in \mathbb{R}^{N \times d}$, at cost $\mathcal{O}(Ndm)$. Aggregation over $\mathcal{A}^{(l)}$ then costs $\mathcal{O}(m|\mathcal{A}^{(l)}|)$ per layer. The output layer with $\Phi \in \mathbb{R}^{m \times c}$ requires $\mathcal{O}(Nmc)$. Putting these together for an L -layer network and assuming $B \ll |\mathbf{A}^l|$ for all l , the overall complexity is $\mathcal{O}(LNdm + \sum_{l=1}^L |\mathcal{A}^{(l)}| \log |\mathcal{A}^{(l)}|)$.

C More Experimental Results

C.1 Configures

We construct a series of experiments to assess the proposed TorqueGNN. Our model is implemented in PyTorch on a workstation with AMD Ryzen 9 5900X CPU (3.70GHz), 64GB RAM and RTX 3090GPU (24GB caches). Our code is available at <https://anonymous.4open.science/r/TorqueGNN-F60C/README.md>.

C.2 Datasets

- **Homophilous Datasets.** Citeseer, Cora and Pubmed are three citation networks, and they are published in [58]. Specifically,
 - **Citeseer** comprises 3,327 publications classified into six categories, with each paper encoded by a 3,703-dimensional binary word-presence vector.
 - **Cora** consists of 2,708 scientific publications classified into seven research topics. Each paper is represented by a 1,433-dimensional binary feature vector indicating the presence of specific word
 - **Pubmed** is a larger citation network of 19,717 diabetes-related articles labeled among three classes. Papers are described by 500-dimensional term frequency-inverse document frequency feature vectors, and citation edges capture scholarly references.
- **Heterophilous Datasets**
 - **Texas, Wisconsin, Cornell** are WebKB datasets used in [59], where nodes correspond to individual web pages and edges correspond to the hyperlinks between them. Every node is described by a bag-of-words feature vector extracted from its page content, and each page has been manually labeled into one of five categories.
 - **Actor** [60] is the actor-only induced subgraph of a film-director-actor-writer network on Wikipedia, where each node represents an actor and an undirected edge connects two actors if they co-occur on the same Wikipedia page.
 - **Tolokers** [61] is built from the Toloka crowdsourcing platform, comprising 11,758 nodes and 519,000 edges that link workers who collaborated on the same task. Each node carries a 10-dimensional feature vector and is assigned one of two labels based on whether the worker was banned.
 - **Questions** [61] is an interaction graph of users on the Yandex Q question-answering platform, comprising 48,921 nodes and 153,540 edges that link users who interacted on the same question. Each node carries a 301-dimensional feature vector and a binary label for node classification.
 - **Penn94** [62] is a subgraph of the Facebook100 dataset featuring 41,554 university students as nodes, connected by 1,362,229 undirected friendship edges. Each node is described by a five-dimensional feature vector and labeled by the gender of the students.

C.3 Methods

C.3.1 GNNs for Homophilous and Heterophilous Graphs

GCN generalize convolutional neural networks to graph-structured data by iteratively aggregating feature information from each node’s local neighborhood,

$$\mathbf{h}_i^{(l)} = \sigma(\tilde{\mathbf{A}}\mathbf{h}_i^{(l-1)}\mathbf{W}^{(l)}), \quad (19)$$

where \mathbf{W} is the learnable parameter matrix.

GAT leverages attention mechanisms to weight the influence of neighboring nodes during message passing. Its core rule is:

$$\mathbf{h}_i^{(l+1)} = \sigma \left(\sum_{j \in \mathcal{N}_i} \alpha_{ij} \mathbf{W} \mathbf{h}_j^{(l)} \right), \alpha_{ij} = \frac{\exp \left(\text{LeakyReLU} \left(a^\top \left[\mathbf{W} \mathbf{h}_i^{(l)} \parallel \mathbf{W} \mathbf{h}_j^{(l)} \right] \right) \right)}{\sum_{k \in \mathcal{N}_i} \exp \left(\text{LeakyReLU} \left(a^\top \left[\mathbf{W} \mathbf{h}_i^{(l)} \parallel \mathbf{W} \mathbf{h}_k^{(l)} \right] \right) \right)}. \quad (20)$$

APPNP first achieves the feature transformation by:

$$\mathbf{H}^{(0)} = \mathbf{XW}, \quad (21)$$

and then propagating message via a Personalized PageRank scheme:

$$\mathbf{H}^{(l)} = (1 - \alpha)\mathbf{PH}^{(l-1)} + \alpha\mathbf{H}^{(0)}. \quad (22)$$

Here, $\mathbf{P} = \mathbf{D}^{-1/2} \mathbf{A} \mathbf{D}^{-1/2}$ is the symmetrically normalized adjacency matrix and α is a trade-off hyperparameter.

H₂GCN contains three designs, and the first design aims to separate ego- and neighbor-message:

$$\mathbf{h}_i^{(l)} = [\mathbf{h}_i^{(l-1)} \parallel \text{Agg}(\{\mathbf{h}_j^{(l-1)} : v_j \in \mathcal{N}_i\})] \quad (23)$$

Second, H₂GCN directly aggregates neighbors of different hops, which enhances high-order information:

$$\mathbf{h}_i^{(l)} = [\mathbf{h}_i^{(l-1)} \parallel \text{Agg}(\{\mathbf{h}_j^{(l-1)} : v_j \in \mathcal{N}_i^1 \parallel \text{Agg}(\{\mathbf{h}_j^{(l-1)} : v_j \in \mathcal{N}_i^2 \parallel \dots\})\})]. \quad (24)$$

Finally, the output is gained by combining the intermediate representations of all layers:

$$\mathbf{h}_i = [\mathbf{h}_i^{(1)} \parallel \mathbf{h}_i^{(2)} \parallel \dots \parallel \mathbf{h}_i^{(L)}]. \quad (25)$$

GPR-GNN generalizes personalized PageRank by treating each hop’s contribution as a learnable parameter:

$$\mathbf{H} = \sum_{l=1}^L \gamma^l \mathbf{P} \mathbf{H}^{(0)}, \mathbf{H}^{(0)} = \mathbf{H} \mathbf{W}, \quad (26)$$

where $\gamma^l \mathbf{P}$ measures the propagation coefficient for the connection between nodes v_i and v_j .

FAGCN adaptively balances low- and high-frequency graph signals via a learnable mixing coefficient:

$$\mathbf{h}_i^{(l)} = \eta \mathbf{h}_i^{(0)} + \sum_{j \in \mathcal{N}_i} \frac{\alpha_{ij}}{\sqrt{d_i d_j}} \eta \mathbf{h}_i^{(l-1)}, \quad (27)$$

where $\alpha_{ij} \in (-1, 1)$ is a learnable coefficient.

ACM-GNN dynamically learns how to weight multiple propagation channels:

$$\mathbf{H}^{(l)} = \text{ReLU} \left(\text{diag} \left(\alpha_H^{(l)} \right) (\mathbf{I} - \mathbf{P}) \mathbf{H}^{(l-1)} \mathbf{W}_H^{(l)} + \text{diag} \left(\alpha_L^{(l)} \right) \mathbf{P} \mathbf{H}^{(l-1)} \mathbf{W}_L^{(l)} + \text{diag} \left(\alpha_I^{(l)} \right) \mathbf{H}^{(l-1)} \mathbf{W}_I^{(l)} \right). \quad (28)$$

Here, α is adaptive mixing weight.

OGNN introduces an order-aware message passing by sorting neighbors according to learned importance scores before aggregation:

$$\mathbf{h}_i = \mathbf{h}_i^{(1)} \odot g_i^{(1)} + \mathbf{h}_i^{(2)} \odot (g_i^{(2)} - g_i^{(1)}) \dots + \mathbf{h}_i^{(L)} \odot (g_i^{(KL)} - g_i^{(L-1)}), \quad (29)$$

where $g_i^{(l)}$ is a vector with a split point $p_i^{(l)}$ so that its first entries are 0 and its remaining entries are 1.

M2MGNN partitions neighbor embeddings into class-aligned “chunks” via learnable soft labels:

$$\mathbf{h}_i^{(l)} = \text{ReLU} \left((1 - \beta) \mathbf{h}_i^{(0)} + \beta \mathbf{m}_i^{(l)} \right), \mathbf{C}_{it}^{(l)} = \sum_{j \in \mathcal{N}_i} \mathbf{s}_t^{(l)}(i, j) \hat{\mathbf{h}}_j^{(k)}, \quad \mathbf{m}_i^{(l)} = \parallel_{t=1}^C \mathbf{C}_{it}^{(l)}, \quad (30)$$

where $\mathbf{s}_t^{(l)}(i, j)$ is the score of node v_i towards v_j in the t -th chunk.

PCNet introduces a unified two-fold filtering framework that simultaneously performs homophilous low-pass smoothing and heterophilous high-pass aggregation:

$$\mathbf{H} = \left(\sum_{k=1}^K \theta_k \text{PC}_k(\tilde{L}) + \theta_0 \right) \mathbf{X} \mathbf{W}. \quad (31)$$

Here, $\text{PC}_k(\tilde{L})$ denotes the n -th Poisson–Charlier polynomial of the normalized Laplacian \tilde{L} , and $\{\theta_k\}_{k=0}^K$ are learnable filter coefficients.

C.3.2 Rewiring Strategies

FoSR develops a spectral-expansion-based rewiring algorithm that adds edges to alleviate over-squashing, and integrates it with a relational GNN to provably avoid oversmoothing.

JDR simultaneously refines graph topology and node features by aligning the principal eigenspaces of their matrices, boosting GNNs across both homophilous and heterophilous networks.

DropEdge randomly removes edges at each training epoch to act as both data augmentation and message-passing reduction, which is used to mitigate over-fitting and over-smoothing problems.

C.4 Hyperparameters

In the subsection, we list the detailed hyperparameters used for the experiments and they are also provided in code. The hyperparameters can be found in Table 4.

Table 4: Hyperparameters of TorqueGNN in 10 datasets.

| Datasets | Lr | Wd | Dropout | L | t | r | epochs |
|-----------|-------|------|---------|-----|-----|-----|--------|
| Texas | 0.001 | 5e-4 | 0.7 | 8 | 5 | 0.2 | 100 |
| Wisconsin | 0.001 | 0.5 | 0.5 | 8 | 5 | 0.2 | 100 |
| Cornell | 0.001 | 0.05 | 0.7 | 8 | 2 | 0.2 | 100 |
| Actor | 0.001 | 0.05 | 0.1 | 8 | 5 | 0.2 | 100 |
| Citeseer | 0.001 | 5e-8 | 0.1 | 8 | 2 | 0.2 | 100 |
| Cora | 0.001 | 0.1 | 0.1 | 8 | 2 | 0.2 | 100 |
| Pubmed | 0.001 | 0.08 | 0.1 | 12 | 5 | 0.2 | 100 |
| Tolokers | 0.001 | 5e-8 | 0.1 | 2 | 2 | 0.2 | 500 |
| Questions | 0.001 | 5e-8 | 0.1 | 2 | 2 | 0.2 | 500 |
| Penn94 | 0.001 | 5e-8 | 0.1 | 2 | 2 | 0.2 | 500 |

C.5 Experiments

Ablation Study. To validate the effectiveness of our proposed torque metric, we conduct ablation studies comparing three edge-scoring schemes. As reported in Table 5, reliance on structural distance alone yields the poorest classification performance on most benchmarks, reflecting the fact that certain long-range connections convey meaningful semantics. Introducing the energy metric markedly improves accuracy, confirming its significance as a measure of edge perturbation strength. Moreover, on Tolokers and Pubmed, the energy-only variant achieves the highest accuracy, slightly surpassing the combined torque score, likely because some low-interference connections carrying critical semantic information are inadvertently pruned when the distance is too large. Crucially, our torque score, integrating both distance and energy, consistently outperforms either criterion besides Tolokers and Pubmed, thereby validating its superior ability to accurately identify disruptive edges, guide interference-aware rewiring, and enhance overall classification accuracy.

Parameter Sensitivity. Figure 5 explores the effect of network depth L . Across most datasets, performance peaks at $L = 8$, thereby validating the effectiveness of our THR strategy for mining high-order information. Beyond eight layers, accuracy declines, primarily due to training challenges typical of deep networks, such as over-smoothing. While our rewiring mechanism mitigates over-smoothing to some extent, it is not explicitly engineered to resolve this phenomenon; overcoming depth-related bottlenecks remains a direction for future work.

D Broader Impact Statement and Limitations

This study aims to enhance message passing in graph neural networks through graph rewiring. As a result, it contributes to better performance and broader applicability of GNNs across a wide range of

Table 5: Ablation Study: Performance of TorqueGNN equipped with different edge-scoring metrics; the best results are shown in bold.

| Datasets | Distance | Energy | Torque (Distance \times Energy) |
|-----------|--------------|---------------------|-----------------------------------|
| Texas | 88.61 (0.70) | 89.16 (0.69) | 91.11 (1.67) |
| Wisconsin | 79.20 (2.40) | 84.60 (1.80) | 89.60 (1.20) |
| Cornell | 81.94 (4.17) | 83.05 (0.83) | 89.44 (1.67) |
| Actor | 36.69 (0.40) | 35.48 (0.07) | 36.72 (0.16) |
| Tolokers | 72.46 (0.04) | 76.11 (0.28) | 75.28 (0.02) |
| Penn94 | 81.11 (0.09) | 81.20 (0.15) | 81.30 (0.19) |
| Questions | 63.11 (1.26) | 62.65 (0.53) | 63.54 (0.85) |
| Citeseer | 73.35 (0.24) | 76.53 (0.42) | 76.84 (0.60) |
| Cora | 78.30 (0.59) | 84.50 (0.00) | 85.39 (0.30) |
| Citeseer | 73.35 (0.24) | 76.53 (0.42) | 76.84 (0.60) |
| Pubmed | 88.01 (0.11) | 88.52 (0.16) | 88.36 (0.08) |

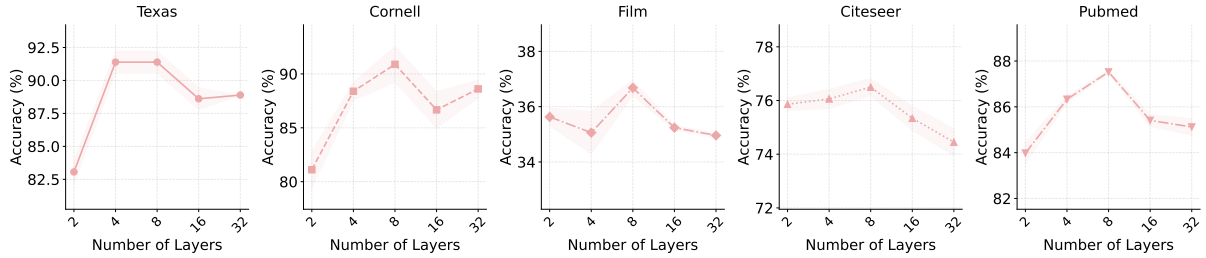


Figure 5: Parameter sensitivity: Performance curves on five datasets with layers changing in $\{2, 4, 8, 16, 32\}$.

tasks, including recommendation systems, molecular property prediction, traffic forecasting, and social network.

THR depends on sorting operations that impose considerable computational and memory burdens on large, densely connected graphs. Additionally, by assigning equal weight to distance and energy metrics, THR may inadvertently prune edges that carry essential semantic information and exhibit low interference when the distance is too large. How to optimally balance these two metrics in accordance with the characteristics of different datasets remains an open challenge.

References

- [1] V. Gligorijević, P. D. Renfrew, T. Kosciolk, J. K. Leman, D. Berenberg, T. Vatanen, C. Chandler, B. C. Taylor, I. M. Fisk, H. Vlamakis, *et al.*, “Structure-based protein function prediction using graph convolutional networks,” *Nature communications*, vol. 12, no. 1, p. 3168, 2021.
- [2] J. Xia, L. Zhang, X. Zhu, Y. Liu, Z. Gao, B. Hu, C. Tan, J. Zheng, S. Li, and S. Z. Li, “Understanding the limitations of deep models for molecular property prediction: Insights and solutions,” *Advances in Neural Information Processing Systems*, vol. 36, pp. 64774–64792, 2023.
- [3] H. Chen, Y. Bei, Q. Shen, Y. Xu, S. Zhou, W. Huang, F. Huang, S. Wang, and X. Huang, “Macro graph neural networks for online billion-scale recommender systems,” in *Proceedings of the ACM web conference 2024*, pp. 3598–3608, 2024.
- [4] V. Anand and A. K. Maurya, “A survey on recommender systems using graph neural network,” *ACM Transactions on Information Systems*, vol. 43, no. 1, pp. 1–49, 2025.
- [5] J. Jiang, C. Han, W. X. Zhao, and J. Wang, “Pdformer: Propagation delay-aware dynamic long-range transformer for traffic flow prediction,” in *Proceedings of the AAAI conference on artificial intelligence*, pp. 4365–4373, 2023.

- [6] R. Liu, Y. Wang, H. Xu, J. Sun, F. Zhang, P. Li, and Z. Guo, “Vul-lmgns: Fusing language models and online-distilled graph neural networks for code vulnerability detection,” *Information Fusion*, vol. 115, p. 102748, 2025.
- [7] S. Huang, Y. Pi, T. Zhang, W. Liu, and Z. Cui, “Boosting graph convolution with disparity-induced structural refinement,” in *Proceedings of the ACM on Web Conference 2025*, pp. 2209–2221, 2025.
- [8] L. Zhang, D. Xu, A. Arnab, and P. H. Torr, “Dynamic graph message passing networks,” in *Proceedings of the IEEE/CVF Conference on Computer Vision and Pattern Recognition*, pp. 3726–3735, 2020.
- [9] Y. Yang, J. Yang, R. Bao, D. Zhan, H. Zhu, X. Gao, H. Xiong, and J. Yang, “Corporate relative valuation using heterogeneous multi-modal graph neural network,” *IEEE Trans. Knowl. Data Eng.*, vol. 35, no. 1, pp. 211–224, 2023.
- [10] C. Qian, A. Manolache, K. Ahmed, Z. Zeng, G. V. den Broeck, M. Niepert, and C. Morris, “Probabilistically rewired message-passing neural networks,” in *The Twelfth International Conference on Learning Representations*, pp. 1–26, 2024.
- [11] P. W. Battaglia, J. B. Hamrick, V. Bapst, A. Sanchez-Gonzalez, V. Zambaldi, M. Malinowski, A. Tacchetti, D. Raposo, A. Santoro, R. Faulkner, *et al.*, “Relational inductive biases, deep learning, and graph networks,” *arXiv preprint arXiv:1806.01261*, 1806.
- [12] R. Xue, H. Han, M. Torkamani, J. Pei, and X. Liu, “Lazygcn: Large-scale graph neural networks via lazy propagation,” in *International Conference on Machine Learning*, pp. 38926–38937, 2023.
- [13] R. Abboud, R. Dimitrov, and I. I. Ceylan, “Shortest path networks for graph property prediction,” in *Learning on Graphs Conference*, pp. 5–1, 2022.
- [14] J. Gasteiger, S. Weissenberger, and S. Günnemann, “Diffusion improves graph learning,” *Advances in neural information processing systems*, vol. 32, 2019.
- [15] L. Yang, M. Li, L. Liu, C. Wang, X. Cao, Y. Guo, *et al.*, “Diverse message passing for attribute with heterophily,” *Advances in Neural Information Processing Systems*, vol. 34, pp. 4751–4763, 2021.
- [16] Y. Zheng, H. Zhang, V. Lee, Y. Zheng, X. Wang, and S. Pan, “Finding the missing-half: Graph complementary learning for homophily-prone and heterophily-prone graphs,” in *International Conference on Machine Learning*, pp. 42492–42505, 2023.
- [17] S. Y. Lee, F. Bu, J. Yoo, and K. Shin, “Towards deep attention in graph neural networks: Problems and remedies,” in *International conference on machine learning*, pp. 18774–18795, 2023.
- [18] L. Page, S. Brin, R. Motwani, and T. Winograd, “The pagerank citation ranking: Bringing order to the web,” tech. rep., Stanford infolab, 1999.
- [19] I. M. Kloumann, J. Ugander, and J. Kleinberg, “Block models and personalized pagerank,” *Proceedings of the National Academy of Sciences*, vol. 114, no. 1, pp. 33–38, 2017.
- [20] W.-Q. Tang, X. Yi, H. Guan, X.-W. Wang, Y.-W. Gu, Y.-J. Zhao, J. Fu, W. Li, Y. Cheng, S.-S. Meng, *et al.*, “Bipolar molecular torque wrench modulates the stacking of two-dimensional metal–organic framework nanosheets,” *Journal of the American Chemical Society*, vol. 145, no. 49, pp. 26580–26591, 2023.
- [21] S. Dzhimak, A. Svidlov, A. Elkina, E. Gerasimenko, M. Baryshev, and M. Drobotenko, “Genesis of open states zones in a dna molecule depends on the localization and value of the torque,” *International Journal of Molecular Sciences*, vol. 23, no. 8, p. 4428, 2022.
- [22] M. I. Drobotenko, A. A. Svidlov, A. A. Dorohova, M. G. Baryshev, and S. S. Dzhimak, “Medium viscosity influence on the open states genesis in a dna molecule,” *Journal of Biomolecular Structure and Dynamics*, vol. 43, no. 5, pp. 2253–2261, 2025.
- [23] S. Kovarik, R. Schlitz, A. Vishwakarma, D. Ruckert, P. Gambardella, and S. Stepanow, “Spin torque-driven electron paramagnetic resonance of a single spin in a pentacene molecule,” *Science*, vol. 384, no. 6702, pp. 1368–1373, 2024.

- [24] M. Camarasa-Gómez, D. Hernangómez-Pérez, and F. Evers, “Spin-orbit torque in single-molecule junctions from ab initio,” *The Journal of Physical Chemistry Letters*, vol. 15, no. 21, pp. 5747–5753, 2024.
- [25] F. Wu, A. H. S. Jr., T. Zhang, C. Fifty, T. Yu, and K. Q. Weinberger, “Simplifying graph convolutional networks,” in *Proceedings of the Thirty-Sixth International Conference on Machine Learning*, pp. 6861–6871, 2019.
- [26] M. Chen, Z. Wei, Z. Huang, B. Ding, and Y. Li, “Simple and deep graph convolutional networks,” in *International conference on machine learning*, pp. 1725–1735, 2020.
- [27] S. Xu, J. Han, Y. Liu, H. Liu, and Y. Bai, “Few-shot traffic classification based on autoencoder and deep graph convolutional networks,” *Scientific Reports*, vol. 15, no. 1, p. 8995, 2025.
- [28] A. Deac, M. Lackenby, and P. Veličković, “Expander graph propagation,” in *Learning on Graphs Conference*, pp. 38–1, 2022.
- [29] R. B. Gabrielsson, M. Yurochkin, and J. Solomon, “Rewiring with positional encodings for graph neural networks,” *Transactions on Machine Learning Research*, 2023.
- [30] H. Shirzad, A. Velingker, B. Venkatachalam, D. J. Sutherland, and A. K. Sinop, “Expformer: Sparse transformers for graphs,” in *International Conference on Machine Learning*, pp. 31613–31632, 2023.
- [31] K. Karhadkar, P. K. Banerjee, and G. Montúfar, “Fosr: First-order spectral rewiring for addressing oversquashing in gnns,” *arXiv preprint arXiv:2210.11790*, 2022.
- [32] P. K. Banerjee, K. Karhadkar, Y. G. Wang, U. Alon, and G. Montúfar, “Oversquashing in gnns through the lens of information contraction and graph expansion,” in *2022 58th Annual Allerton Conference on Communication, Control, and Computing (Allerton)*, pp. 1–8, 2022.
- [33] J. Topping, F. Di Giovanni, B. P. Chamberlain, X. Dong, and M. M. Bronstein, “Understanding over-squashing and bottlenecks on graphs via curvature,” *arXiv preprint arXiv:2111.14522*, 2021.
- [34] F. Di Giovanni, L. Giusti, F. Barbero, G. Luise, P. Lio, and M. M. Bronstein, “On over-squashing in message passing neural networks: The impact of width, depth, and topology,” in *International conference on machine learning*, pp. 7865–7885, 2023.
- [35] J. H. Giraldo, K. Skianis, T. Bouwmans, and F. D. Malliaros, “On the trade-off between over-smoothing and over-squashing in deep graph neural networks,” in *Proceedings of the 32nd ACM international conference on information and knowledge management*, pp. 566–576, 2023.
- [36] J. Linkerhägner, C. Shi, and I. Dokmanic, “Joint graph rewiring and feature denoising via spectral resonance,” *CoRR*, vol. abs/2408.07191, 2024.
- [37] Y. Yan, M. Hashemi, K. Swersky, Y. Yang, and D. Koutra, “Two sides of the same coin: Heterophily and oversmoothing in graph convolutional neural networks,” in *IEEE International Conference on Data Mining (ICDM)*, pp. 1287–1292, 2022.
- [38] S. Luan, C. Hua, Q. Lu, J. Zhu, M. Zhao, S. Zhang, X.-W. Chang, and D. Precup, “Revisiting heterophily for graph neural networks,” *Advances in neural information processing systems*, vol. 35, pp. 1362–1375, 2022.
- [39] D. Bo, X. Wang, C. Shi, and H. Shen, “Beyond low-frequency information in graph convolutional networks,” in *Proceedings of the AAAI conference on artificial intelligence*, vol. 35, pp. 3950–3957, 2021.
- [40] L. Liang, S. Kim, K. Shin, Z. Xu, S. Pan, and Y. Qi, “Sign is not a remedy: Multiset-to-multiset message passing for learning on heterophilic graphs,” *arXiv preprint arXiv:2405.20652*, 2024.
- [41] P. Veličković, G. Cucurull, A. Casanova, A. Romero, P. Lio, and Y. Bengio, “Graph attention networks,” in *Proceedings of the Sixth International Conference on Learning Representations*, pp. 1–12, 2018.

- [42] M. Ranzato, Y. Boureau, S. Chopra, and Y. LeCun, “A unified energy-based framework for unsupervised learning,” in *Proceedings of the Eleventh International Conference on Artificial Intelligence and Statistics*, pp. 371–379, 2007.
- [43] W. Grathwohl, K. Wang, J. Jacobsen, D. Duvenaud, M. Norouzi, and K. Swersky, “Your classifier is secretly an energy based model and you should treat it like one,” in *Proceedings of the 8th International Conference on Learning Representations*, 2020.
- [44] Q. Wu, Y. Chen, C. Yang, and J. Yan, “Energy-based out-of-distribution detection for graph neural networks,” in *The Eleventh International Conference on Learning Representations*, pp. 1–18, 2023.
- [45] E. Jang, S. Gu, and B. Poole, “Categorical reparameterization with gumbel-softmax,” in *Proceedings of the 5th International Conference on Learning Representations*, OpenReview.net, 2017.
- [46] G. Wan, Z. Shi, W. Huang, G. Zhang, D. Tao, and M. Ye, “Energy-based backdoor defense against federated graph learning,” in *The Thirteenth International Conference on Learning Representations*, pp. 1–30, 2025.
- [47] J. Klicpera, A. Bojchevski, and S. Günnemann, “Predict then propagate: Graph neural networks meet personalized pagerank,” in *Proceedings of the Seventh International Conference on Learning Representations*, pp. 1–15, 2019.
- [48] A. Hyvärinen, J. Hurri, P. O. Hoyer, A. Hyvärinen, J. Hurri, and P. O. Hoyer, “Estimation of non-normalized statistical models,” *Natural Image Statistics: A Probabilistic Approach to Early Computational Vision*, pp. 419–426, 2009.
- [49] A. Hyvärinen and P. Dayan, “Estimation of non-normalized statistical models by score matching,” *Journal of Machine Learning Research*, vol. 6, no. 4, 2005.
- [50] T. N. Kipf and M. Welling, “Semi-supervised classification with graph convolutional networks,” in *Proceedings of the Fifth International Conference on Learning Representations*, pp. 1–13, 2017.
- [51] J. Zhu, Y. Yan, L. Zhao, M. Heimann, L. Akoglu, and D. Koutra, “Beyond homophily in graph neural networks: Current limitations and effective designs,” *Advances in neural information processing systems*, vol. 33, pp. 7793–7804, 2020.
- [52] E. Chien, J. Peng, P. Li, and O. Milenkovic, “Adaptive universal generalized pagerank graph neural network,” *arXiv preprint arXiv:2006.07988*, 2020.
- [53] Y. Song, C. Zhou, X. Wang, and Z. Lin, “Ordered GNN: ordering message passing to deal with heterophily and over-smoothing,” in *The Eleventh International Conference on Learning Representations*, pp. 1–18, 2023.
- [54] B. Li, E. Pan, and Z. Kang, “Pc-conv: Unifying homophily and heterophily with two-fold filtering,” in *Proceedings of the Thirty-Eighth AAAI Conference on Artificial Intelligence*, pp. 13437–13445, 2024.
- [55] K. Karhadkar, P. K. Banerjee, and G. Montúfar, “Fosr: First-order spectral rewiring for addressing oversquashing in gnns,” *arXiv preprint arXiv:2210.11790*, 2022.
- [56] Y. Rong, W. Huang, T. Xu, and J. Huang, “Dropedge: Towards deep graph convolutional networks on node classification,” *arXiv preprint arXiv:1907.10903*, 2019.
- [57] D. Zugner and S. Günnemann, “Adversarial attacks on graph neural networks via meta learning,” in *Proceedings of the International Conference on Learning Representations*, 2019.
- [58] P. Sen, G. Namata, M. Bilgic, L. Getoor, B. Galligher, and T. Eliassi-Rad, “Collective classification in network data,” *AI magazine*, vol. 29, no. 3, pp. 93–93, 2008.
- [59] H. Pei, B. Wei, K. C.-C. Chang, Y. Lei, and B. Yang, “Geom-gcn: Geometric graph convolutional networks,” *arXiv preprint arXiv:2002.05287*, 2020.
- [60] J. Tang, J. Sun, C. Wang, and Z. Yang, “Social influence analysis in large-scale networks,” in *Proceedings of the 15th ACM SIGKDD international conference on Knowledge discovery and data mining*, pp. 807–816, 2009.

- [61] O. Platonov, D. Kuznedelev, M. Diskin, A. Babenko, and L. Prokhorenkova, “A critical look at the evaluation of gnns under heterophily: Are we really making progress?,” *arXiv preprint arXiv:2302.11640*, 2023.
- [62] D. Lim, F. Hohne, X. Li, S. L. Huang, V. Gupta, O. Bhalerao, and S. N. Lim, “Large scale learning on non-homophilous graphs: New benchmarks and strong simple methods,” *Advances in neural information processing systems*, vol. 34, pp. 20887–20902, 2021.